Electronic Supplementary Material (ESI) for Sustainable Energy & Fuels.

Supporting Information for

In Situ Formation of Highly Exposed $NiPS_3$ Nanosheets on Nickel Foam as Efficient 3D Electrocatalyst for Overall Water Splitting

Liang Fang[a, *], Yanping Xie[b], Peiyin Guo[b], Jingpei Zhu[a], Shuhui Xiao[a], Shujie Sun[a], Wei Zi[a], Hongbin Zhao[c]

a. Collaborative Innovation Center of Henan Province for Energy-Saving Building Materials Xinyang Normal University, Xinyang, Henan, 464000, P.R. China

b. Analysis & Testing Center, Xinyang Normal University, Xinyang, Henan, 464000, China

c. College of Sciences, Shanghai University, Shanghai 200444, China

***Corresponding author.**

Tel: +86-376-6370838.

E-mail address: fangliang@xynu.edu.cn (L. Fang)

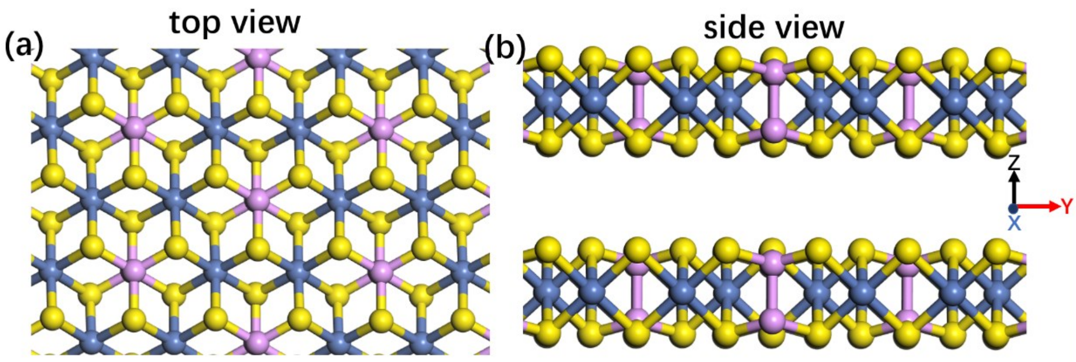

Figure S1. The corresponding $NiPS_3$ crystal structure from the top view in the plane of (001) and the side view of $NiPS_3$.

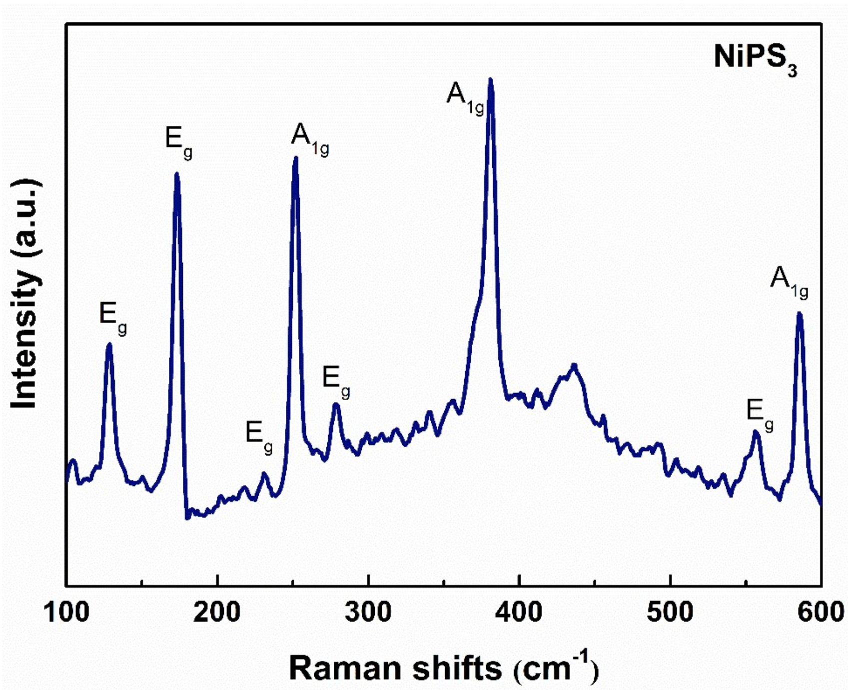

Figure S2. Raman spectra of prepared $NiPS_3$ nanosheets.

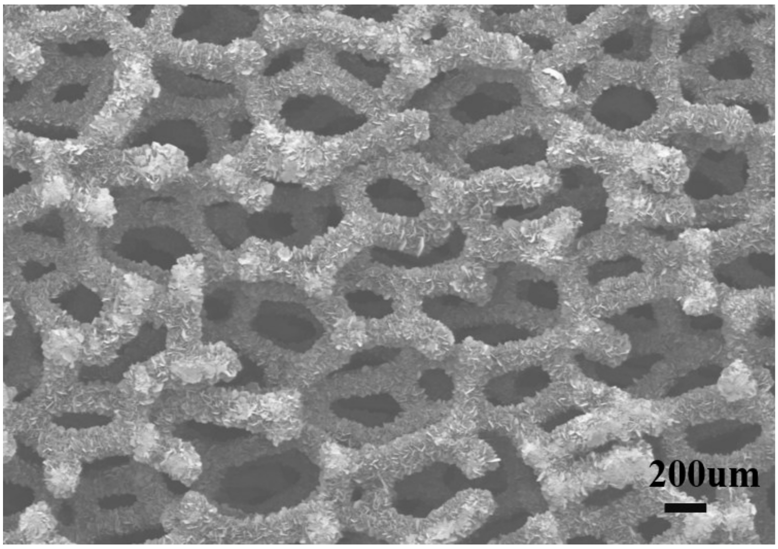

Figure S3. The low-magnification SEM image of $NiPS_3$/Ni.

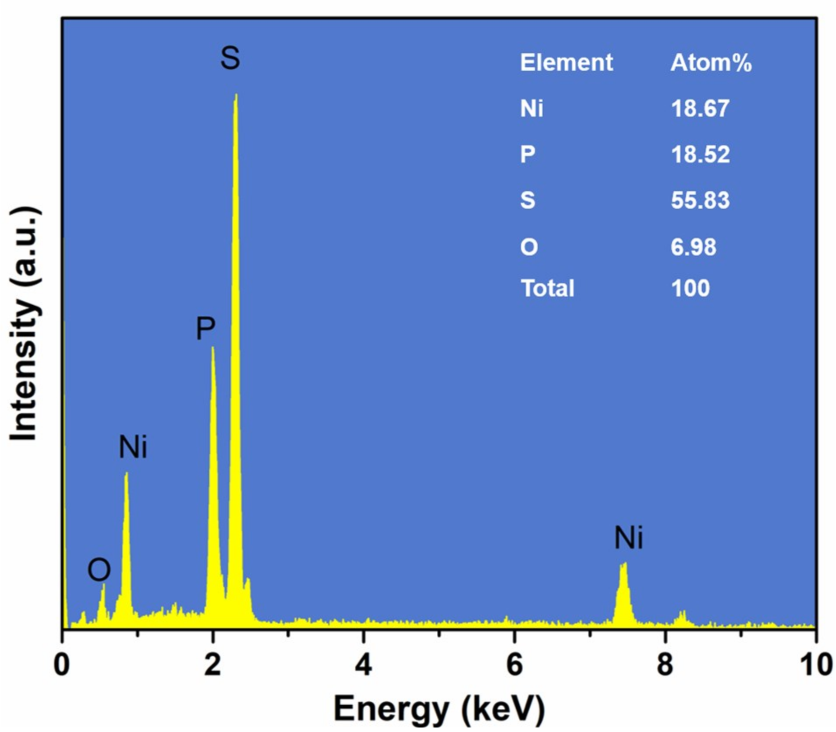

Figure S4. EDX spectrum of $NiPS_3$ nanosheets.

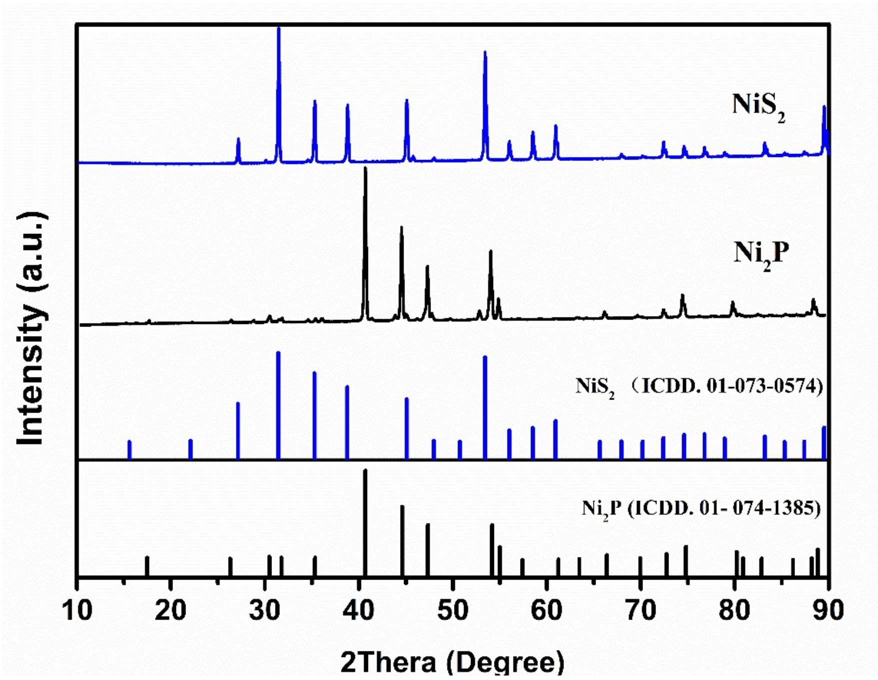

Figure S5. XRD patterns of the as-prepared Ni_2P/Ni and NiS_2/Ni.

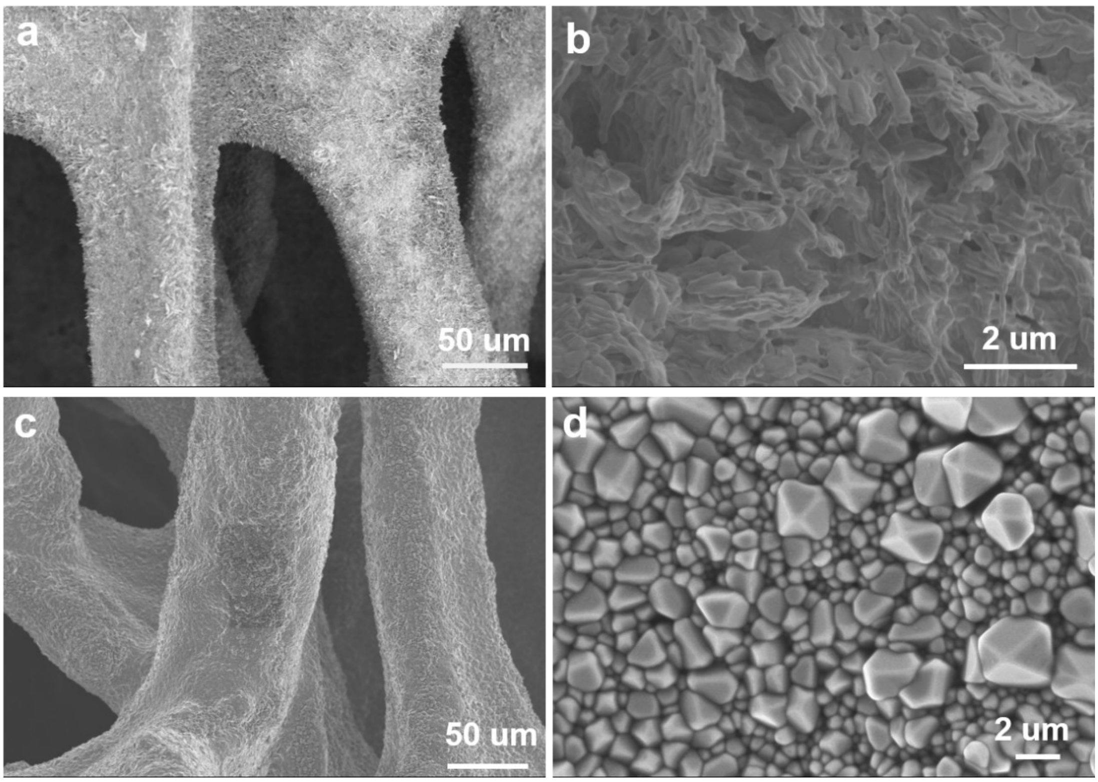

Figure S6. SEM images of the as-prepared Ni_2P/Ni (a,b) and NiS_2/Ni (c,d).

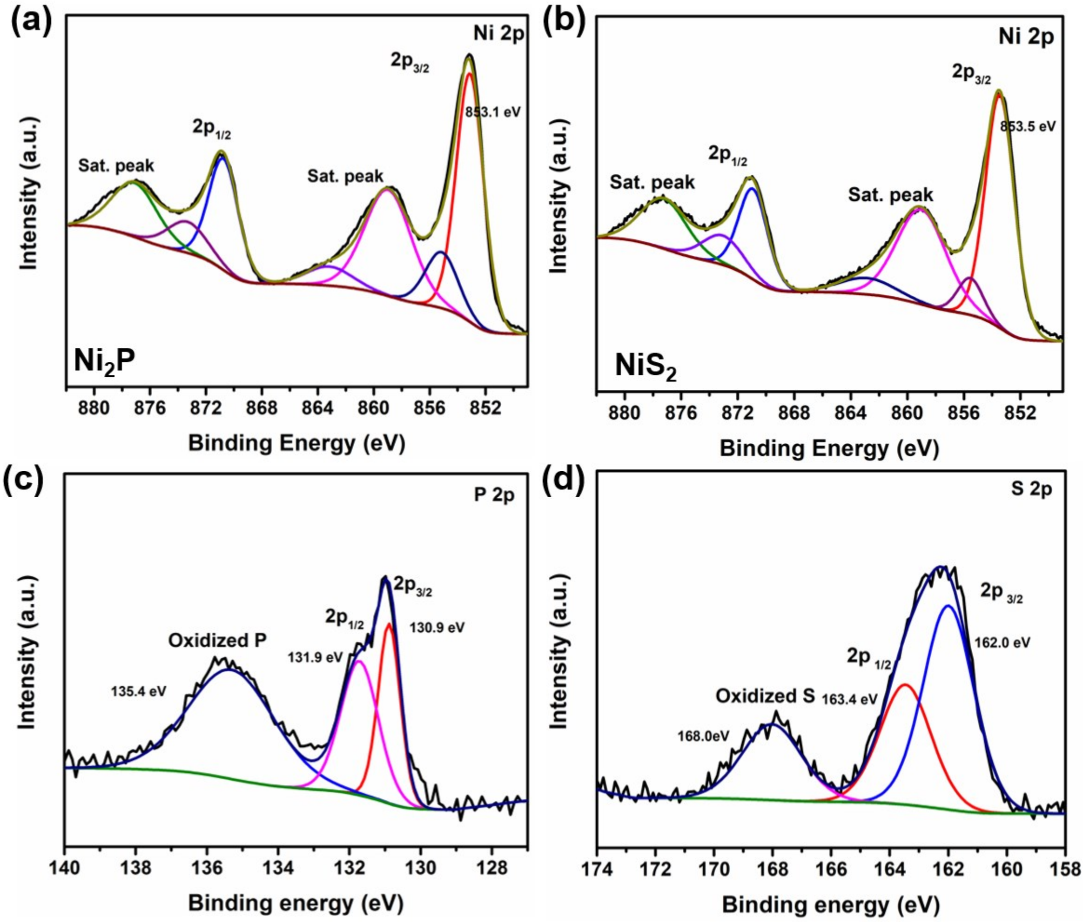

Figure S7. The high resolution of the (a) Ni 2p, (c) P 2p of Ni_2P. The high resolution of the (b) Ni 2p, (d) S 2p of NiS_2.

Table S1. HER performance of $NiPS_3$/Ni as compared to other state-of-the-art MPS_3 catalysts and transition metal-based catalysts in alkaline electrolyte.

Catalysts	**η_{10} (mV)**	**Tafel slopes** mV dec^{-1}	**References**
$NiPS_3$/Ni	74	86	This work
$Ni_{0.9}Fe_{0.1}PS_3$	72	73	1
$Fe_2P_2S_6$ NCs	175	137	2
$Ni_{1-x}Co_xPS_3$ NSs	71	77	3
$NiP_{0.62}S_{0.38}$	54	52.3	4
FeP_2 NW arrays	189	67	5
CoS_x-Ni_3S_2/NF	146@20 mA cm^{-2}	141	6
$Ni_{0.9}Fe_{0.1}PS_3$@MXene	196	114	7
NMoNi/SWCNT	130	128	8
CoP/CC	209	129	9
Ni_2P	250@20 mA cm^{-2}	100	10
C,N-doped $NiPS_3$	53.2	38.2	11
Few-layer $NiPS_3$	398	48	12
$NiCoPS_3$/C nanosheets	140	60	13
rGO-few-layer $FePS_3$	192		14

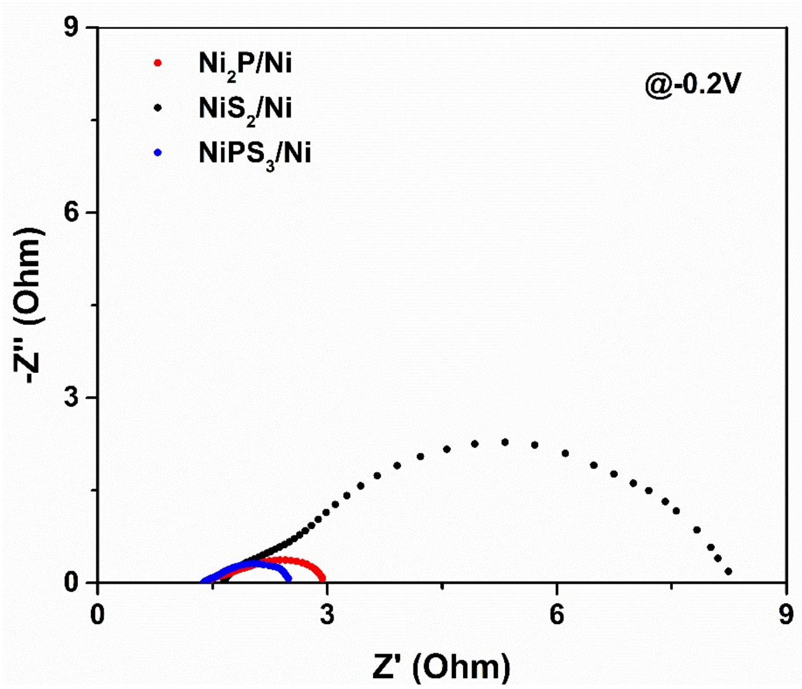

Figure S8. Nyquist plots of the $NiPS_3$/Ni, Ni_2P/Ni and NiS_2/Ni catalysts.

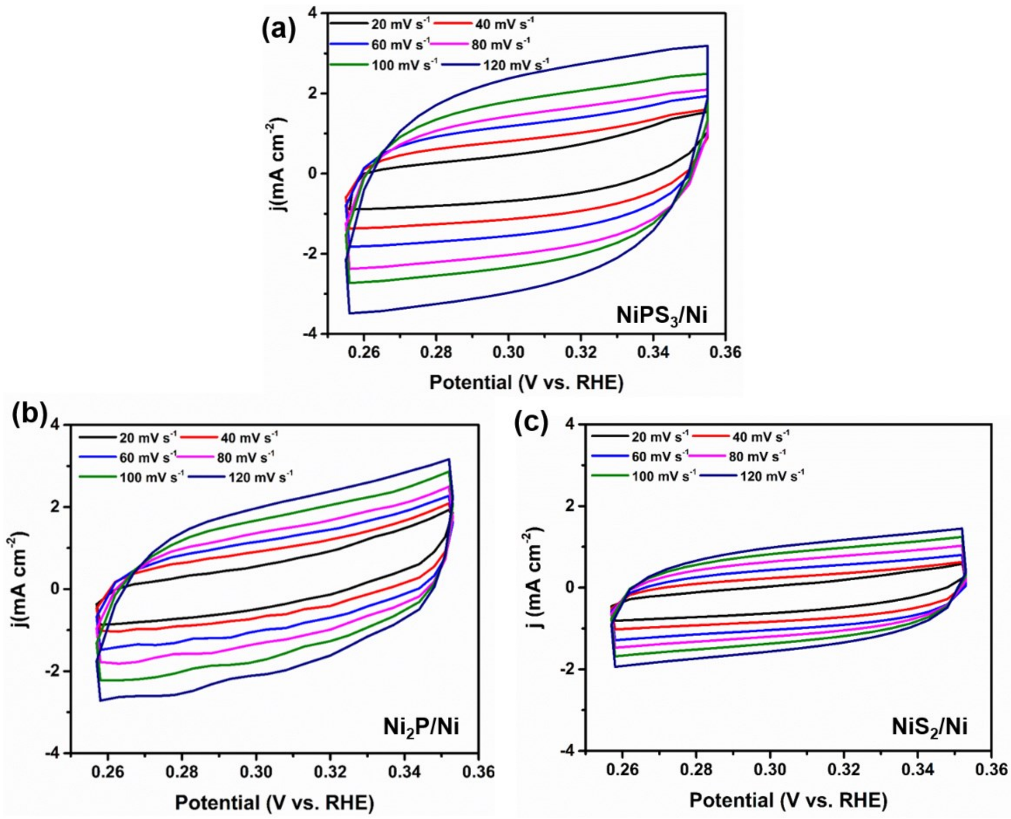

Figure S9. CV curves at a potential range of 0.257 V - 0.355V in 1 M KOH for (a) $NiPS_3$/Ni, (b) Ni_2P/Ni, and (c) NiS_2/Ni. Scan rates of 20, 40, 60, 80, 100, and 120 mV s^{-1} were used.

The obtained specific capacitance is converted into the ESCA according to the specific capacitance value of a flat standard material with a real surface area of 1cm^{-2}. Literatures reported that the specific capacitance value of a flat surface is usually in the range of 20~60μF•cm^{-2}. In this work, we presume the standard capacitance value of the flat surface as 40 μF•cm^{-2} for the following calculations of ESCA.

According to the ESCA calculation equation of the catalyst:

$$ESCA = \frac{C_{dl}}{C_s}$$

Where C_{dl} is the double layer capacitance, and C_s is the standard capacitance value of the flat surface. As a result, the ESCAs of $NiPS_3$, Ni_2P and NiS_2 were calculated to be 477, 380 and 232 cm^{-2}.

$$n_{H_2} = \left(j\frac{mA}{cm^2}\right)\cdot\left(\frac{1C\cdot S^{-1}}{1000mA}\right)\cdot\left(\frac{1mol\ e^-}{96485.3C}\right)\cdot\left(\frac{1mol\ H_2}{2mol\ e^-}\right)\cdot\left(\frac{6.022\times10^{23}H_2\ molecules}{1\ mol\ H_2}\right)$$

$$= 3.12\times10^{15}\frac{H_2/S}{cm^2}per\frac{mA}{cm^2}$$

Due to the exact hydrogen bonding sites are not known, we assume that all the exposed atoms including Ni, P and S atoms can serve as the active sites. The total number of surface sites were assessed from the unit cells of $NiPS_3$, Ni_2P and NiS_2.

$$n^{surface\ sites}_{NiPS3} = \left(\frac{20\ atoms\ per\ unit\ cell}{371.23\ Å^3 per\ unit\ cell}\right)^{2/3} = 1.426\times10^{15}\ atoms\cdot cm^{-2}_{real}$$

$$n^{surface\ sites}_{Ni2P} = \left(\frac{9\ atoms\ per\ unit\ cell}{100.54\ Å^3 per\ unit\ cell}\right)^{2/3} = 2.001\times10^{15}\ atoms\cdot cm^{-2}_{real}$$

$$n^{surface\ sites}_{NiS2} = \left(\frac{12\ atoms\ per\ unit\ cell}{183.73\ Å^3 per\ unit\ cell}\right)^{2/3} = 1.622\times10^{15}\ atoms\cdot cm^{-2}_{real}$$

Finally, plot of current density can be converted into the TOF plot based on the following formula:

$$TOF_{NiPS3} = \frac{\left(3.12\times10^{15}\frac{H_2/S}{cm^2}per\frac{mA}{cm^2}\right)\times|j|}{surface\ sites\ \times A_{ESCA}} = 0.0046\times|j|$$

$$TOF_{Ni2P} = \frac{(3.12 \times 10^{15} \frac{H_2/S}{cm^2} per \frac{mA}{cm^2}) \times |j|}{surface\ sites\ \times A_{ESCA}} = 0.0041 \times |j|$$

$$TOF_{NiS2} = \frac{(3.12 \times 10^{15} \frac{H_2/S}{cm^2} per \frac{mA}{cm^2}) \times |j|}{surface\ sites\ \times A_{ESCA}} = 0.0083 \times |j|$$

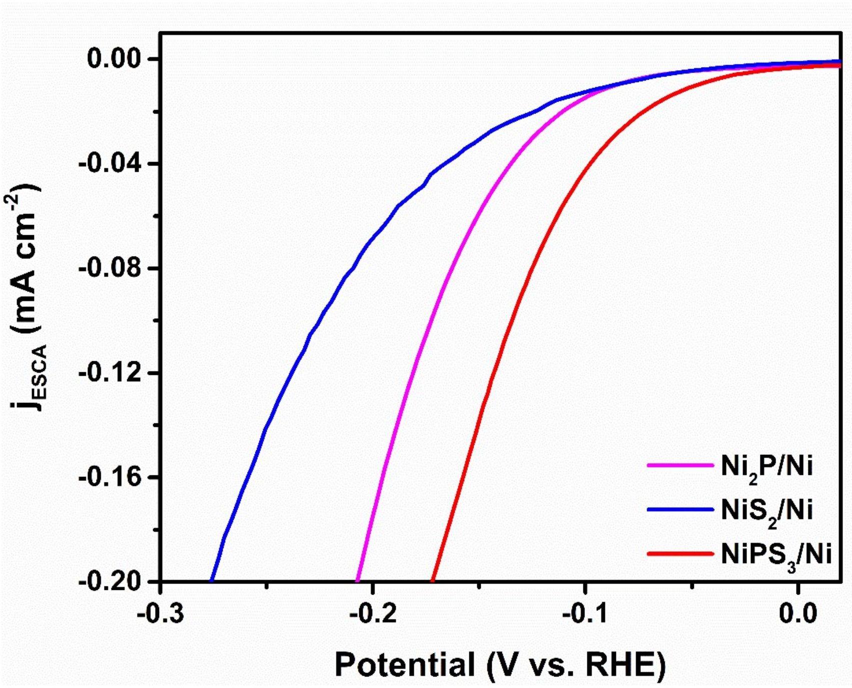

Figure S10. Polarization curves with current density normalized by ESCA for $NiPS_3/Ni$, Ni_2P/Ni and NiS_2/Ni.

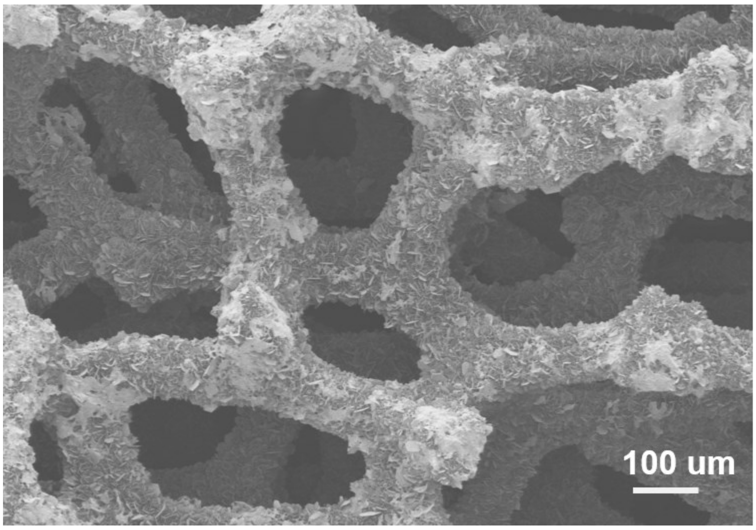

Figure S11. SEM image of $NiPS_3$/Ni after HER stability. After 10h HER, the vertically-aligned $NiPS_3$ nanosheets on Ni foam still be well preserved, indicating a good stability for $NiPS_3$/Ni.

Due to improved electron transfer between $NiPS_3$ nanosheets and Ni foam, the catalysis activity on the surface of 2D nanosheets is efficiently enhanced. To confirm this, the electrodeposition of Ag nanoparticles on the surface of $NiPS_3$ nanosheets was carried out in 0.1 mM $AgNO_3$ solution. A three-electrode set-up was used with the $NiPS_3$/Ni as working electrode, Pt wire as counter electrode and saturated calomel reference electrode (SCE). After electrodeposited at a constant potential of -0.2 V vs SCE for 100s, we observed the Ag nanoparticles were easily deposited on the basal surface of $NiPS_3$ nanosheets (Figure S10). This observation further suggested the 2D $NiPS_3$ nanosheets directly attachment to the conducting Ni foam can provide efficient electron transport along the basal facet of 2D nanosheets, which will facilitate the H adsorption during HER process and enhance the intrinsic activity of $NiPS_3$.

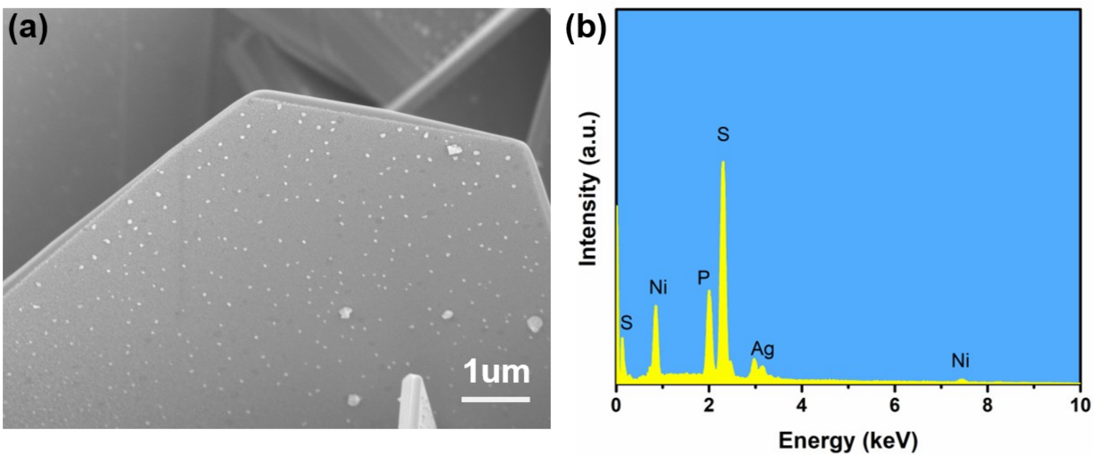

Figure S12. (a) SEM image of $NiPS_3$/Ni with Ag particles deposited. (b) EDX spectrum from the corresponding elemental of Ni, P, S, and Ag. The Ag nanoparticles were mainly deposited on the (001) facets, further suggesting the electrons are readily available for the reduction reaction on the basal surface of $NiPS_3$ nanosheets.

Table S2. OER performance of $NiPS_3/Ni$ as compared to other state-of-the-art MPS_3 catalysts and transition metal-based catalysts in alkaline electrolyte.

Catalysts	η_{10} (mV)	Tafel slopes mV dec^{-1}	References
$NiPS_3/Ni$	273	77	This work
$NiPS_3$	440mV @20 mA cm^{-2}	73	1
$Fe_2P_2S_6$ NCs	288	45.6	2
$NiP_{0.62}S_{0.38}$	240	46	4
$Ni_{0.7}Fe_{0.3}PS_3$@MXene	282	36.5	7
$NiPS_3$@NiOOH	350	80	15
NiMnOP/NF	189	29.2	16
$Co_{0.8}Fe_{0.2}P$	270	50	17
Ni-Fe (O_xH_y)	298	37	18
Co_xFeP_x/C	260	58	19
CoPS	301.8	58	20
$NiPS_3$@Graphene	294	42.6	21
Few-layer $NiPS_3$ nanosheets	300mV @20 mA cm^{-2}	43	22
NiSe@NiOOH/NF	332mV @50 mA cm^{-2}	162	23
NiCoFe phosphide	270	65	24

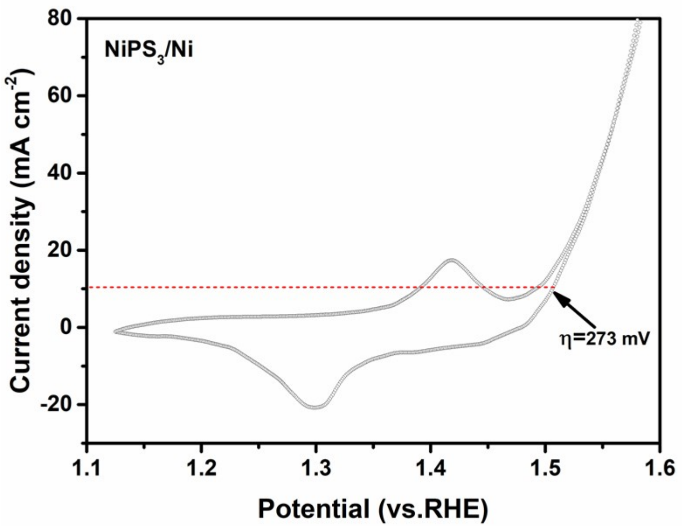

Figure S13. CV curve of $NiPS_3$/Ni recorded at 2 mV s^{-1}.

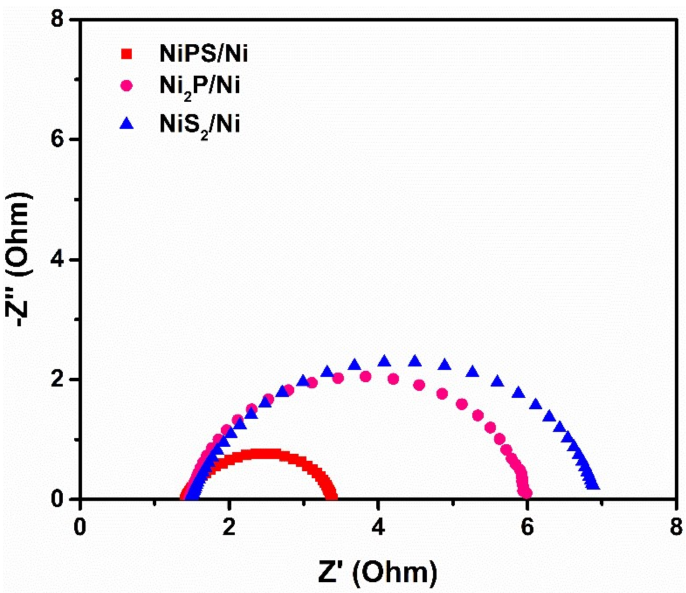

Figure S14. Nyquist plots of $NiPS_3$/Ni, Ni_2P/Ni and NiS_2/Ni electrodes.

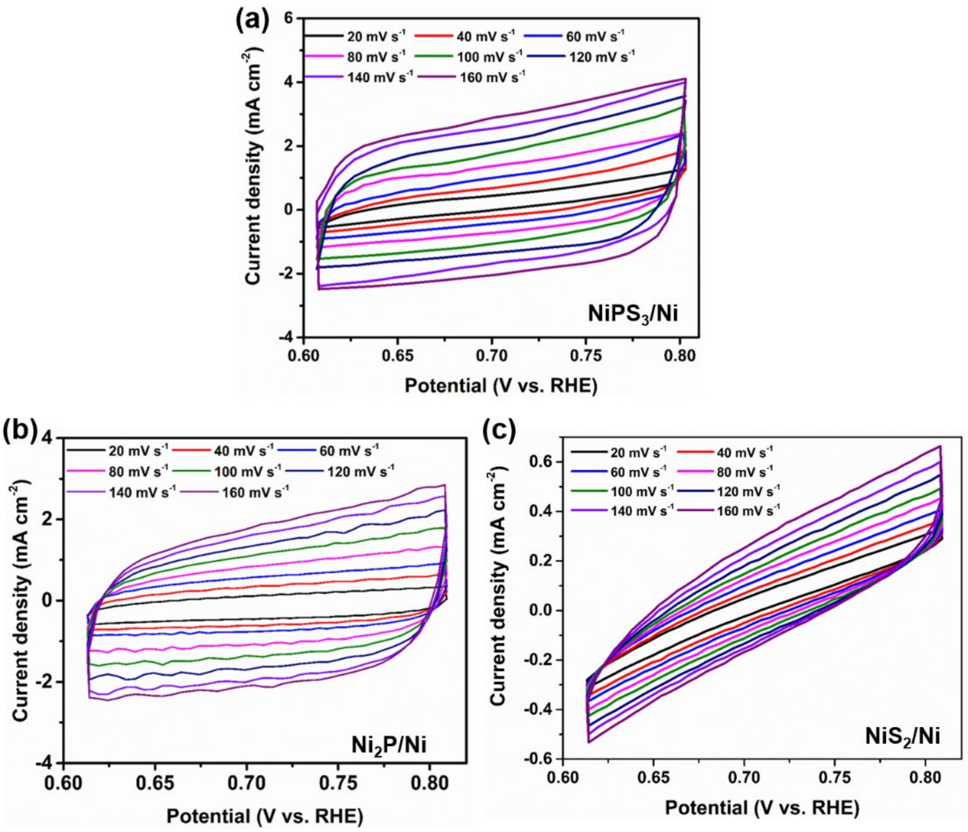

Figure S15. CV curves at a potential range of 0.607 V - 0.803V in 1 M KOH for (a) $NiPS_3$/Ni, (b) Ni_2P/Ni, and (c) NiS_2/Ni. Scan rates of 20, 40, 60, 80, 100, 120, 140, and 160 mV s^{-1} were used.

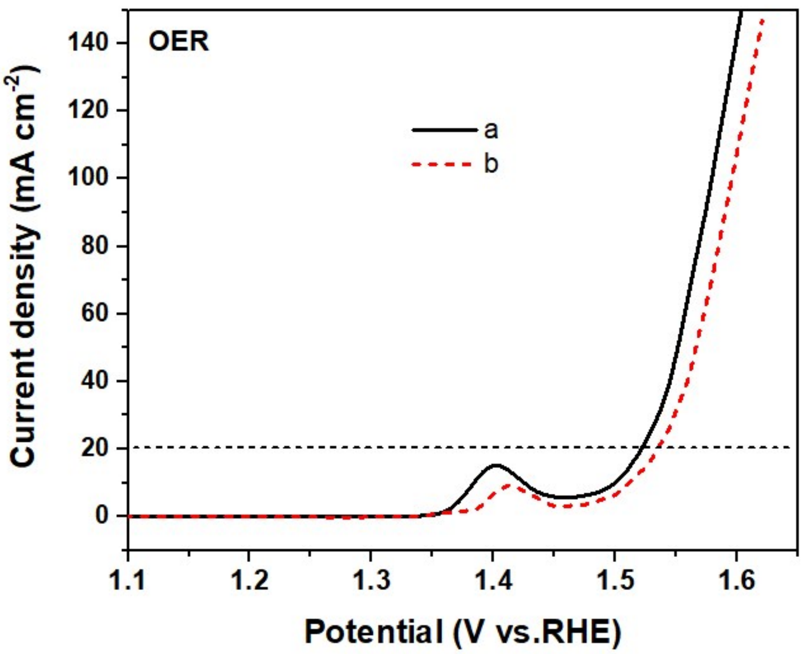

Figure S16. LSV curves after CV scans in the region of (a) 0.75~1.60 V and (b) 0.75~1.36 V *vs*. RHE, respectively.

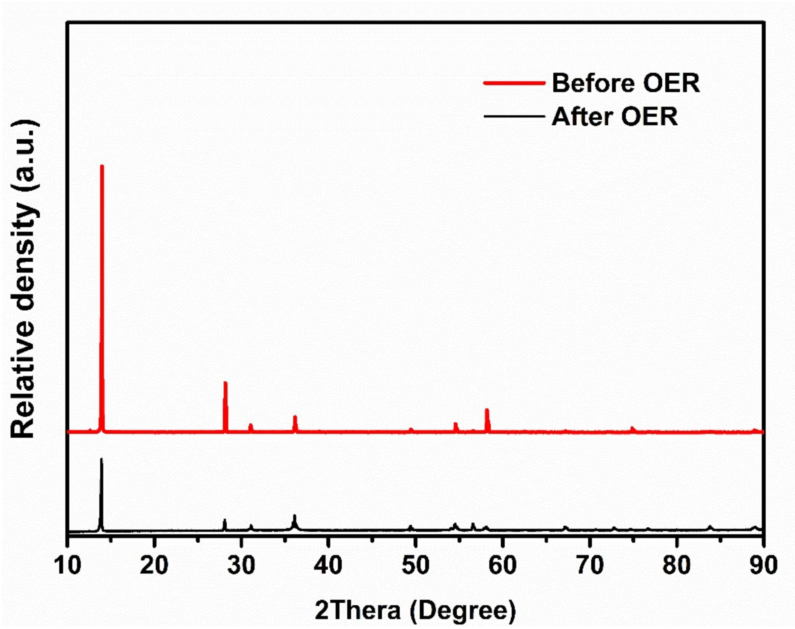

Figure S17. XRD patterns of the $NiPS_3$/Ni before and after OER for 6h.

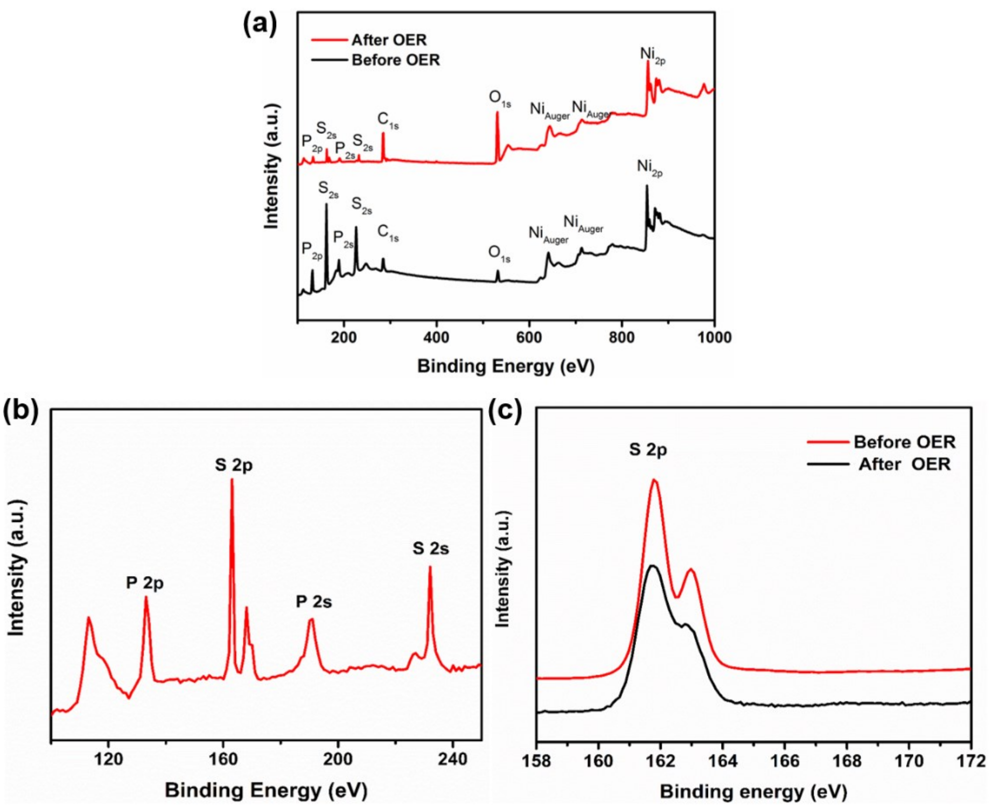

Figure S18. (a) XPS survey spectrum of $NiPS_3$/Ni before and after OER. (b) XPS spectra after OER, highlighting the presence of P and S in $NiPS_3$. (c) A comparison of the S 2p core level spectra of $NiPS_3$ before and after the OER.

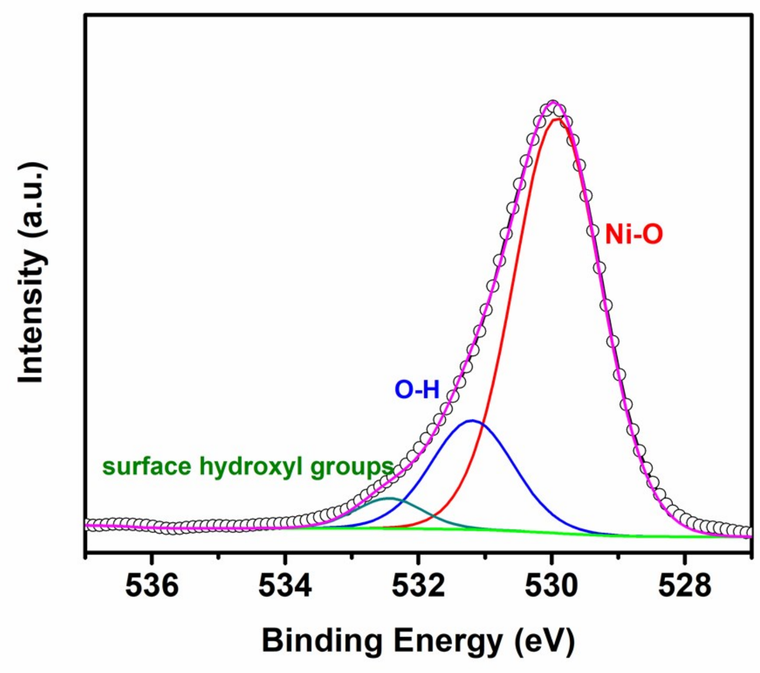

Figure S19. O1s XPS spectrum for $NiPS_3$ after OER.

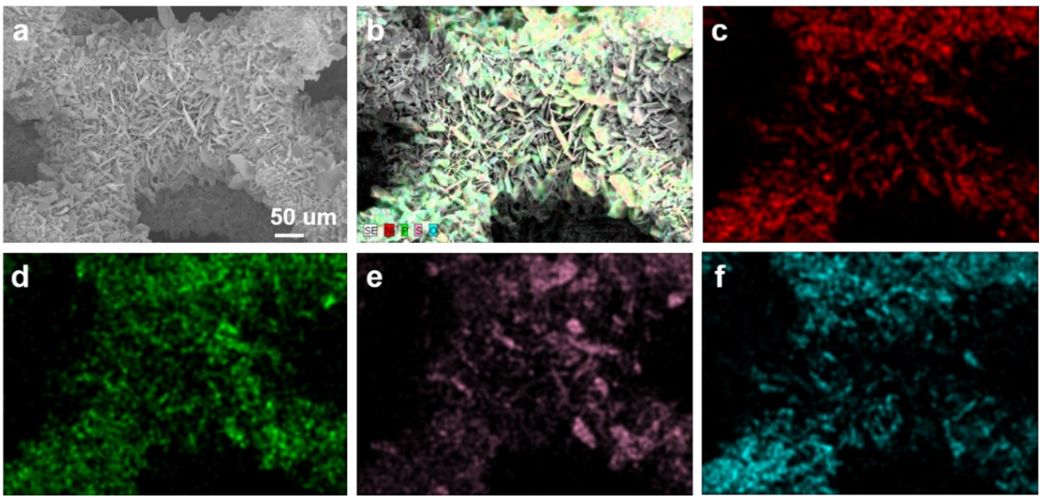

Figure S20. The SEM elemental distribution mapping of Ni, P, S, and O elements for $NiPS_3$/Ni electrode after OER.

References

1.B. Song, K. Li, Y. Yin, T. Wu, L.N. Dang, M. Cabán-Acevedo, J.C. Han, T.L. Gao, X.J. Wang, Z.H. Zhang, J.R. Schmidt, P. Xu, S. Jin, Tuning Mixed Nickel Iron Phosphosulfide Nanosheet Electrocatalysts for Enhanced Hydrogen and Oxygen Evolution, *ACS. Catal.* **2017**, 7, 8549-8557.

2. J.F. Chang, G.Z. Wang, A. Belharsa, J.J. Ge, W. Xing, Y. Yang, Stable $Fe_2P_2S_6$

Nanocrystal Catalyst for High-Efficiency Water Electrolysis, *Small Methods* **2019**, 1900632.
3. K. Li, D. Rakov, W. Zhang, P. Xu, Improving the Intrinsic Electrocatalytic Hydrogen Evolution Activity of Few-layer $NiPS_3$ by Cobalt Doping, *Chem. Commun.* **2017**, 53, 8199-8202.
4. J. Guo, H.Y. Wang, G. Su, Y.L. Tang, H.Q. Liu, F.Y. Tian, D.L. Li, Self-Supported Nickel Phosphosulphide Nanosheets for Highly Efficient and Stable Overall Water Splitting, *J. Mater. Chem. A* **2017**, 5, 14865-14872.
5. C.Y. Song, I.H. Kwak, Y.R. Lim, J. Park, FeP and FeP_2 Nanowires for Efficient Electrocatalytic Hydrogen Evolution Reaction, *Chem. Commun.* **2016**, 52, 2819-2822.
6. L.W. Jiang, N. Yang, C.X. Yang, X.Y. Zhu, Y.N. Jiang, X.P. Shen, C.C. Li, Q.F. Sun, Surface Wettability Engineering: CoS_x-Ni_3S_2 Nanoarray Electrode for Improving Overall Water Splitting, *Appl. Catal. B: Environ.* **2020**, 269, 118780.
7. C.F. Du, K.N. Dinh, Q.H. Liang, Y. Zheng, Y.B. Luo, J.L. Zhang, Q.Y. Yan, Self-Assemble and In Situ Formation of $Ni_{1-x}Fe_xPS_3$ Nanomosaic-Decorated MXene Hybrids for Overall Water Splitting, *Adv. Energy Mater.* **2018**, 1801127.
8. A. Majeed, X. Li, P.X. Hou, H. Tabassum, L.L. Zhang, C. Liu, H.M. Cheng, Monolayer Carbon-encapsulated Mo-doped Ni Nanoparticles Anchored on Single-wall Carbon Nanotube Film for Total Water Splitting, *Appl. Catal. B:- Environm.* **2020**, 269, 118823.
9. J. Tian, Q. Liu, A. M. Asiri, X. Sun, Self-supported Nanoporous Cobalt Phosphide Nanowire Arrays: an Efficient 3D Hydrogen-evolving Cathode over the Wide Range of PH 0−14, *J. Am. Chem. Soc.* **2014**, 136, 7587-7590.
10. L. Feng, H. Vrubel, M. Bensimon, X. Hu, Easily-prepared Dinickel Phosphide (Ni_2P) Nanoparticles as an Efficient and Robust Electrocatalyst for Hydrogen Evolution,
Phys. Chem. Chem. Phys. **2014**, *16*, 5917.
11. J. Wang, X.Z. Li, B. Wei, R. Sun, W. Yu, H.Y. Hah, H.M. Xu, J. Li, X.B. Ge, Z.X. Chen, C.L. Su, Z.C. Wang, Activating Basal Planes of $NiPS_3$ for Hydrogen Evolution by Nonmetal Heteroatom Doping, *Adv. Funct. Mater.* **2020**, 12, 1908708.
12. R. N. Jenjeti, M. P. Austeria, S. Sampath, Alternate to Molybdenum Disulfide: A 2D, Few-Layer Transition-Metal Thiophosphate and Its Hydrogen Evolution Reaction Activity over a Wide pH Range, *ChemElectroChem* **2016**, *3*, 1392.
13. Q. Liang, L. Zhong, C. Du, Y. Zheng, Y. Luo, J. Xu, S. Li, Q. Yan, Mosaic-Structured Cobalt Nickel Thiophosphate Nanosheets Incorporated N-doped Carbon for Efficient and Stable Electrocatalytic Water Splitting, *Adv. Funct. Mater.* **2018**, *28*, 1805075.

14. D. Mukherjee, P. M. Austeria, S. Sampath, Two-Dimensional, Few-Layer Phosphochalcogenide, $FePS_3$: A New Catalyst for Electrochemical Hydrogen Evolution over Wide pH Range, *ACS Energy Lett.* **2016**, 1, 367.
15. B. Konkena, J. Masa, A.J.R. Botz, I. Sinev, W. Xia, J. Koβmann, R. Drautz, M. Muhler, W. Schuhmanm, Metallic $NiPS_3$@NiOOH Core-shell Heterostructures as Highly Efficient and Stable Electrocatalyst for the Oxygen Evolution Reaction, *ACS Catal.* **2017**, 7, 229-237.
16. J. Balamurugan, T.T. Nguyen, V. Aravindan, N.H. Kim, J.H. Lee, Highly Reversible Water Splitting Cell Building from Hierarchical 3D Nickel Manganese Oxyphosphide Nanosheets, *Nano Energy* **2020**, 69, 104432.
17. M. Jiang, J. Li, J.M. Li, Y. Zhao, L.J. Pan, Q.Q. Cao, D.H. Wang, Y.W. Du, Two-dimensional Bimetallic Phosphide Ultrathin Nanosheets as Non-noble Electrocatalysts for a Highly Efficient Oxygen Evolution Reaction, *Nanoscale* **2019**, 11, 9654.
18. M. Görlin, P. Chernev, P. Paciok, C-W. Tai, J.F.D. Araújo, T. Reier, M. Heggen, R. Dunin-Borkowski, P. Strasser, H. Dau, Formation of Unexpectedly Active Ni–Fe Oxygen Evolution Electrocatalysts by Physically Mixing Ni and Fe Oxyhydroxides, *Chem. Commun.* **2019**, 55, 518.
19. J. Han, G. Chen, X.H. Liu, N. Zhang, S.Q. Liang, R.Z. Ma, G.Z. Qiu, Cobalt Iron Phosphide Nanoparticles Embedded within a Carbon Matrix as Highly Efficient Electrocatalysts for the Oxygen Evolution Reaction, *Chem. Comm.* **2019**, 55, 9212-9215.
20. G.J. Hu, J.X. Xiang, J. Li, P. Liu, R.N. Ali, B. Xiang, Urchin-like Ternary Cobalt Phosphosulfide as High-efficiency and Stable Bifunctional Electrocatalyst for Overall Water Splitting, *Journal of Catalysis* **2019**, 371, 126-134.
21. S. Xue, L. Chen, Z.B. Liu, H.M. Cheng, W.C. Ren, $NiPS_3$ Nanosheet−Graphene Composites as Highly Efficient Electrocatalysts for Oxygen Evolution Reaction, *ACS Nano* **2018**, 12, 5297-5305.
22. R. Dangol, Z. Dai, A. Chaturvedi, Y. Zheng, Y. Zhang, K. N. Dinh, B. Li, Y. Zong, Q.Yan, Few-layer $NiPS_3$ Nanosheets as Bifunctional Materials for Li-ion Storage and Oxygen Evolution Reaction, *Nanoscale* **2018**, 10, 4890-4896.
23. X. Li, G.Q. Han, Y.R. Liu, B. Dong, W.H. Hu, X. Shang, Y.M. Chai, C.G. Liu, NiSe@NiOOH Core−Shell Hyacinth-like Nanostructures on Nickel Foam Synthesized by in Situ Electrochemical Oxidation as an Efficient Electrocatalyst for the Oxygen Evolution Reaction, *ACS Appl. Mater. Interfaces* **2016**, 8, 20057−20066.
24. X.J. Wei, Y.H. Zhang, H.C. He, L. Peng, S.H. Xiao, S.R. Yao, P. Xiao, Carbon-incorporated porous honeycomb NiCoFe phosphide nanospheres derived from a MOF precursor for overall water splitting, *Chem. Commun.* **2019**, 55, 10896-10899.